

MASSACHUSETTS INSTITUTE OF TECHNOLOGY

3.014 Materials Laboratory  
Fall 2005

**LABORATORY 3: Module  $\alpha_1$**

*Radius Ratios and Symmetry in Ionic Crystals*

Instructor: Professor Linn W. Hobbs

**Objectives**

- Discover principles of X-ray diffraction from crystalline materials
- Collect X-ray powder diffraction patterns and analyze using Powder Diffraction File (PDF)
- Explore relationship between relative ion sizes and crystal structure symmetries

**Tasks**

- Calculate structure factors of materials investigated
- Prepare samples for X-ray powder diffraction
- Obtain X-ray powder diffraction patterns for six perovskite-structure oxides
- Compare patterns obtained to calculations and PDF
- Apply peak fitting routines to determine lattice parameters
- Relate composition, lattice parameter, ionic radius, radius ratio, and crystal symmetry

**Materials**

CaTiO<sub>3</sub>, BaTiO<sub>3</sub>, SrTiO<sub>3</sub>, PbTiO<sub>3</sub>, CaZrO<sub>3</sub>, PbZrO<sub>3</sub>

*Introduction*

Many inorganic materials, such as halides like NaCl and oxides like MgO, TiO<sub>2</sub> or Al<sub>2</sub>O<sub>3</sub>, exhibit strong ionic character in their atomic bonding. As a result, atom packing in these systems is dictated by electrostatic forces—the structures chosen by nature are those that maximize interactions between ions of opposite charge while minimizing contact between like-charged ions and maintaining electrical neutrality. Structural consideration of ionic solids begins with the Goldschmidt<sup>1</sup> ionic model, which assumes that ions are essentially charged, incompressible, non-polarizable spheres with a definable radius. As a consequence of electrostatic interactions, ionic crystals create ordered arrangements of coordination polyhedra, in which cations are in contact with a maximum number of surrounding anions, the number depending on the ratio of the cation

radius to the anion radius,  $r_C/r_A$  (Table 1), and to a lesser extent cation charge. A large highly charged cation (such as  $\text{Ba}^{2+}$  or  $\text{U}^{4+}$ ) can accommodate a larger number of anions around it.  $\text{U}^{4+}$  cations in  $\text{UO}_2$  are 8-coordinated by  $\text{O}^{2-}$  anions in the fluorite structure

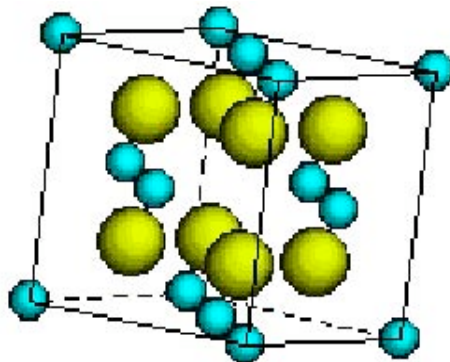


Fig. 1. (8:4) Fluorite structure of  $\text{UO}_2$ , with  $r_C/r_A$  ratio = 0.724. The  $\text{U}^{4+}$  cations form a cubic face-centered arrangement, but alternatively can be thought of as filling *every other* cube interstice in the simple cubic arrangement of  $\text{O}^{2-}$  anions, or as  $[\text{UO}_8]$  coordination cubes linked by sharing edges. In the (4:8) anti-fluorite structure of  $\text{Na}_2\text{O}$ , the roles of anion and cation are reversed, with  $r_A/r_C = 1.39$ ,  $\text{Na}^{2+}$  cations coordinated by four  $\text{O}^{2-}$  anions, and  $[\text{ONa}_8]$  anion coordination cubes sharing edges.

(Fig. 1), while  $\text{Ba}^{2+}$  cations in perovskite-structure  $\text{BaTiO}_3$  (Fig. 4, see below) are 12-coordinated by  $\text{O}^{2-}$  anions). Conversely, smaller and less-highly charged cations cannot accommodate so many anions around them ( $\text{Li}_2\text{O}$  and  $\text{Na}_2\text{O}$  adopt the anti-fluorite structure (Fig. 1) in which the  $\text{Li}^{1+}$  and  $\text{Na}^{1+}$  cations are only 4-coordinated by oxygen).

Table 1. Preferred Cation Coordination in Ionic Crystals

Cation Coordination No.	Anion arrangement	Minimum stable $r_C/r_A$
12	corners of trunc. cube	1.000
8	corners of cube	0.732
6	corners of octahedron	0.414
4	corners of tetrahedron	0.225
3	corners of triangle	0.155
2	collinear	0

Of course, the anion point of view may equally be adopted. In the Na<sub>2</sub>O example just cited, eight (smaller) Na<sup>1+</sup> cations surround each (larger) O<sup>2-</sup> anion. In some cases (like BaO), the cation could accommodate a larger number of anions around it (*e.g.* 8 or 12) than the 6 it has, but the anion cannot accommodate around itself the geometrically consequential number of cations dictated by stoichiometry.

Table 2. *Coordination-Dependent Ionic Radii (Shannon & Prewitt<sup>3</sup>)*

Ion	Radius <i>r</i> (pm) CN = 12	Radius <i>r</i> (pm) CN = 8	Radius <i>r</i> (pm) CN = 6	Radius <i>r</i> (pm) CN = 4
Li <sup>1+</sup>			76	59
Na <sup>1+</sup>		118	102	99
K <sup>1+</sup>	185		138	
Rb <sup>1+</sup>		161	152	
Cs <sup>1+</sup>		177	167	
F <sup>1-</sup>		135	133	
Cl <sup>1-</sup>		184	181	
Mg <sup>2+</sup>			72	
Ca <sup>2+</sup>	134	112	100	
Sr <sup>2+</sup>	144	126	118	
Pb <sup>2+</sup>	149	129	119	
Ba <sup>2+</sup>	161	142	135	
Ti <sup>4+</sup>			61	
Nb <sup>5+</sup>			64	
Zr <sup>4+</sup>			72	
O <sup>2-</sup>		142	140	138

Ionic radii were first computed by the crystal chemist and Nobelist Linus Pauling<sup>2</sup> (also of X-ray crystallography and Vitamin C fame), but revised radii that take into account polarization of the ion cores, and thus depend on coordination, were calculated more recently by Shannon and Prewitt<sup>3</sup> and are those now generally used (Table 2).

Some of the stablest, and therefore most pervasive, ionic structures are those in which radius-ratio criteria are well satisfied for both anions and cations. Classic examples are those binary equiatomic compounds that crystallize in the rocksalt (halite) structure (Fig. 2b)—among them NaCl, KCl, LiF, KBr, CaO, SrO, BaO, CdO, VO,  $\text{Fe}_{1-x}\text{O}$ , CoO, NiO, *etc.*—which have cation:anion radius ratios  $r_c/r_A$  near 0.5 (NaCl 0.563, MgO 0.514) and comprise cation (or anion) coordination octahedra (*e.g.*  $[\text{NaCl}_6]$  octahedra) that share edges. For more similar ion sizes, the CsCl structure is preferred (CsCl itself has  $r_c/r_A = 0.96$ ) in which  $\text{Cs}^{1+}$  ions sit in the centers of cubes of  $\text{Cl}^-$  ions ( $[\text{CsCl}_8]$  cubes) that share faces (Fig. 2).

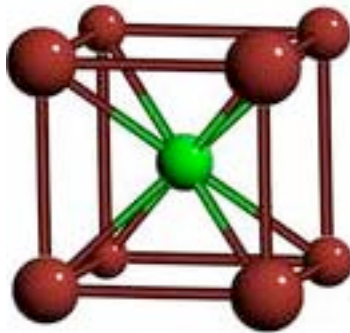


Fig. 2. (8:8) structure of CsCl, in which each ion is 8-coordinated by ions of the opposite charge, may also be thought of as  $[\text{CsCl}_8]$  coordination cubes that share all faces.

Linus Pauling's rules for crystalline compounds (Table 3) codify these notions and provide rationalization for structural tendencies observed in systems with ionic bonding. Despite being couched in terms of ion size, these rules turn out to be essentially driven more by the consideration of minimizing electrostatic energy (which can be accounted in a proper Madelung summation), than by the geometric necessities of ionic radii, however represented.

Table 3. *Pauling's Rules for Crystalline Ionic Compounds*

<p><b>Rule 1. Coordination.</b> A coordination polyhedron of anions is formed around every cation (and <i>vice versa</i>) and is stable <i>only if the cation is in contact with each of its neighboring anions</i>. The distance between anions and cations is thus the sum of the their ionic radii, and the coordination number of the cation will be maximized subject to the criterion of maintaining cation-anion contact.</p>
<p><b>Rule 2. Electrostatic Valency.</b> The total strength of valency “bonds” that reach an anion from all of its neighboring cations equals the charge of the anion.</p>
<p><b>Rule 3. Polyhedral Linking.</b> Cation coordination polyhedra tend to be linked through sharing of anions, at corners first, then edges, then faces—in this order because of the increasing electrostatic repulsion between cations for these successive choices.</p>
<p><b>Rule 4. Cation Evasion.</b> The electrostatic repulsion between cations is greatest for cations of high charge and small coordination number. Thus, in crystals containing different cations, those with higher charge and smaller coordination number are likely to share fewer polyhedral elements.</p>
<p><b>Rule 5. Crystal Homogeneity.</b> The number of structurally distinct sites in a crystalline arrangement of ions tends to be small. This condition ensures that chemically similar atoms experience similar environments.</p>

Ionic radii and radius ratios do *not* actually do a very good job in predicting the structure adopted by a given compound, even in such simple binary compounds as alkali halides, for which Table 1 would predict (4:4) zincblende structure for  $0.225 < r_C/r_A < 0.414$ , (6:6) rocksalt structure for  $0.414 < r_C/r_A < 0.732$ , and (8:8) CsCl structure for  $0.732 < r_C/r_A < 1$ . In actuality, LiF ( $r_C^{IV}/r_A^{IV} = 0.451$ ) only just escapes zincblende structure (the  $\text{Li}^{1+}$  ion does almost rattle around in its cage of six  $\text{F}^{1-}$  ions), but LiBr ( $r_C^{VI}/r_A^{VI} = 0.388$ ) and LiI ( $r_C^{VI}/r_A^{VI} = 0.345$ ), which also adopt the rocksalt structure, are incorrectly predicted to be zincblende. NaF ( $r_C^{VI}/r_A^{VI} = 0.767$ ), KF ( $r_C^{VI}/r_A^{VI} = 1.038$ ), RbF ( $r_C^{VI}/r_A^{VI} = 1.128$ ), and CsF ( $r_C^{VI}/r_A^{VI} = 1.256$ ), all of which adopt the rocksalt structure, are likewise incorrectly predicted to be CsCl. Ionic radii and radius ratios must therefore be used with caution in assessing structural options for compound solids.

Often, ionic crystals can be described alternatively<sup>4</sup> as close packed lattices of anions into which cations are inserted at interstitial sites (Fig. 3a). In this description of

the rocksalt structure of MgO,  $\text{Mg}^{2+}$  cations occupy every octahedral interstice in a cubic close-packed array of  $\text{O}^{2-}$  anions. The corundum structure adopted by  $\alpha\text{-Al}_2\text{O}_3$ , consists

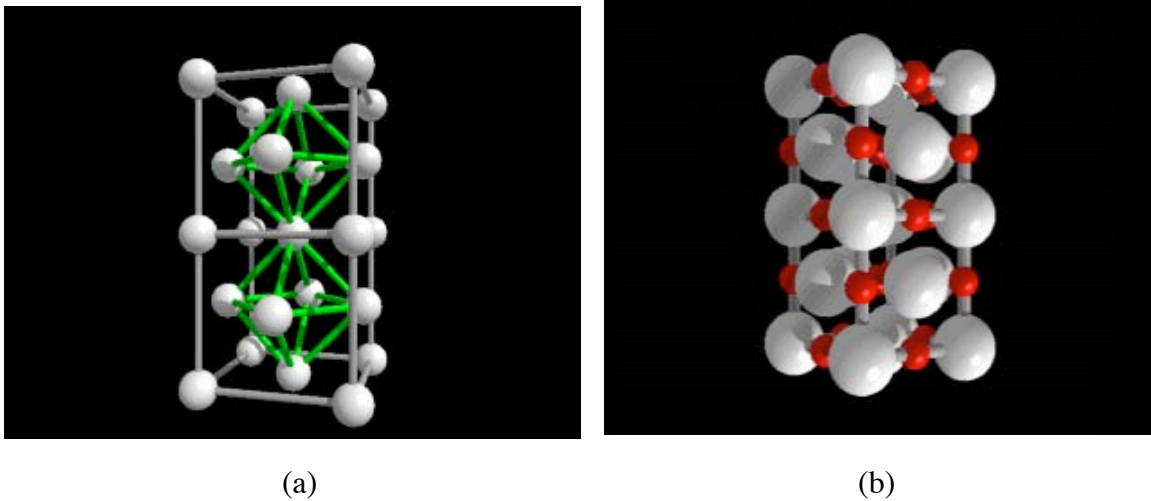


Fig. 3. (a) Octahedral cages (green) surrounding octahedral interstitial sites in a cubic close-packed array of anions. (b) Placement of  $\text{Mg}^{2+}$  cations (red) in every octahedral interstice of a cubic close-packed array of  $\text{O}^{2-}$  anions to form the rocksalt structure adopted by the compound MgO.

of a (nearly) close-packed hexagonal assembly of  $\text{O}^{2-}$  anions, two-thirds of the octahedral interstices of which are occupied by  $\text{Al}^{3+}$  cations. In magnetite,  $\text{Fe}_3\text{O}_4$ , which adopts the (inverse) spinel structure,  $\text{Fe}^{3+}$  cations occupy 1/8 of the tetrahedral interstices and  $\text{Fe}^{2+}$  cations 1/2 the octahedral in a cubic close-packed array of  $\text{O}^{2-}$  anions. Perovskite compounds—the subject of this laboratory experiment, with chemical formulae of the form  $\text{ABO}_3$ —can be thought of as cubic stacking of close-packed layers comprised of  $\text{O}^{2-}$  anions and A-site cations (in the ratio  $\text{AO}_3$ ) in which 1/4 of the octahedral interstices are occupied by B cations. Pauling’s first rule still applies here, in that the cation placed in an interstitial site must not “rattle” around in the interstitial space if it is to stabilize the crystal structure.

The crystalline mineral perovskite ( $\text{CaTiO}_3$ ), from which the associated structural class takes its name, was discovered in the Russian Ural Mountains by Gustav Rose in 1839 and named for the Russian mineralogist L. A. Perovski (1792-1856). A more illuminating description of the idealized perovskite structure involves linking of Pauling’s coordination polyhedra (Fig. 4b) in accordance with Pauling’s rules.  $[\text{TiO}_6]$  octahedra

Figure removed for copyright reasons.

Fig. 4. Two representations of the  $ABO_3$  perovskite structure. a) B-centered representation, showing octahedral cage of  $O^{2-}$  anions surrounding a  $Ti^{4+}$  cation in  $BaTiO_3$ , and b) A-centered representation, with superimposed linkages of  $[TiO_6]$  coordination octahedra, through corner sharing of oxygen anions, that define a large central interstice occupied by the large  $Ba^{2+}$  ion. (Reproduced from W. D. Kingery *et al.*, ref. 4).

comprising small, highly-charged  $Ti^{4+}$  cations surrounded by 6  $O^{2-}$  anions share only corners (unlike  $[MgO_6]$  octahedral in the rocksalt structure, comprising larger, less highly charged  $Mg^{2+}$  cations, which share edges), in keeping with Pauling's third rule, in a cubic arrangement. In this configuration,  $O^{2-}$  anions thus share valency "bonds" with two  $Ti^{4+}$  cations. The arrangement also defines a large interstitial space which can be occupied by a large cation of lower charge, in this case  $Ca^{2+}$ , which is 12-coordinated by  $O^{2-}$  anions in  $[CaO_{12}]$  truncated cubes that share square faces with each other and triangular faces with neighboring  $[TiO_6]$  octahedra, as allowed by Pauling's fourth rule.  $O^{2-}$  anions thus additionally share valency "bonds" with four  $Ca^{2+}$  cations, satisfying Pauling's second rule (the two  $Ti^{4+}$  cations each contribute  $2 \times 4/6 = 16/12$  "valency bonds" and the four  $Ca^{2+}$  cations  $4 \times 2/12 = 8/12$  "valency bonds" to each  $O^{2-}$  anion, for a total of  $24/12 = 2$  "bonds," which equals the ionic charge  $|-2| = 2$  of the  $O^{2-}$  anions). The fact that the ideal crystal structure of perovskite, in fact, satisfies Pauling's Rules rather well implies substantially ionic character to the bonding—although it is known that the Ti-O bond has

significant covalency and Ti is 6-coordinated by O mostly because this maximizes the covalent bonding, not because the ionic radius-ratio  $r_{\text{Ti}^{4+}}/r_{\text{O}^{2-}} = 75 \text{ pm}/126 \text{ pm} = 0.60$  is consistent with octahedral ionic coordination.

The perovskite structure is adopted by a large number of other  $A^{2+}B^{4+}O_3$  compounds, among them (besides  $\text{CaTiO}_3$ )  $\text{SrTiO}_3$ ,  $\text{BaTiO}_3$ ,  $\text{PbTiO}_3$ ,  $\text{PbZrO}_3$  and  $\text{CaZrO}_3$ , which you will study, and additionally compounds such as  $\text{KNbO}_3$  in which a large  $\text{K}^{1+}$  cation is charge-compensated by a small  $\text{Nb}^{5+}$  cation. The radius-ratio criterion (Pauling's first rule) is, however, precisely satisfied only by  $\text{SrTiO}_3$  (which is cubic); other combinations of A and B cations do not ensure that the cations are "in contact" with  $\text{O}^{2-}$  anions. Geometrical contact of hard ion spheres occurs only if  $(r_A + r_O) = \sqrt{2}(r_B + r_O)$ . A structural tolerance parameter<sup>5</sup> can be thus defined

$$t = (r_A + r_O)/\sqrt{2}(r_B + r_O) \quad (1)$$

that defines the limits of 6-fold and 12-fold coordination for the B and A cations in this structure type; the perovskite structure type is stable generally only within the range

Table 4. *Tolerance Parameter for Perovskite Structure Compounds*

$\text{CaZrO}_3$	$\text{CaTiO}_3$	$\text{PbZrO}_3$	$\text{SrTiO}_3$	$\text{PbTiO}_3$	$\text{BaTiO}_3$	$\text{KNbO}_3$
0.914	0.964	0.964	0.999	1.017	1.059	1.127

$0.75 < t < 1.10$  (Table 4). For  $t < 0.90$ , a cooperative buckling of the corner-sharing octahedra occurs that increases the lattice parameter. For  $0.90 < t < 1$ , small distortions or rotations of the octahedra occur (Fig. 5c) that provide cation-anion "contact" but lower the crystal symmetry from cubic to orthorhombic. For  $t > 1$ , highly correlated uniaxial displacements of the B cations occur (Fig. 5a) that convert the cubic symmetry to tetragonal symmetry by selective elongation of one axis. Presence of these distortions, rotations or displacements is easily distinguished by the appearance in diffraction patterns of diffraction maxima that are forbidden (have zero structure factor, see below) for the

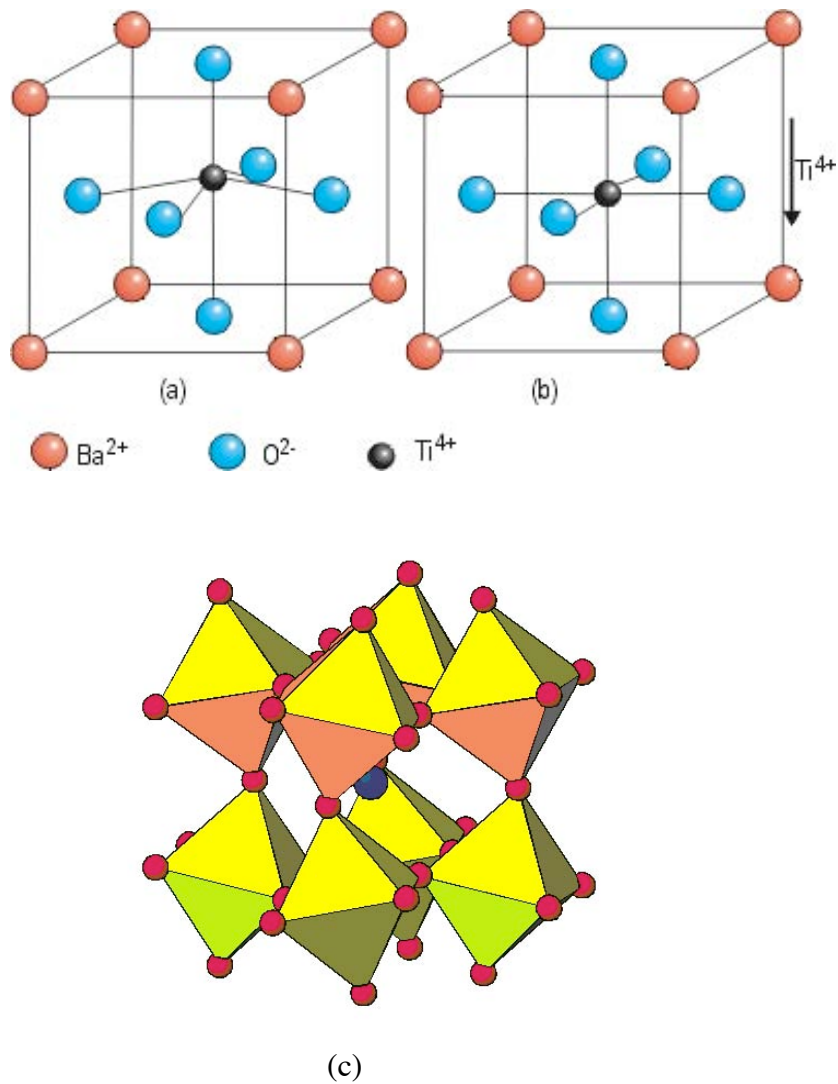


Fig. 5. Distortions of the perovskite structure accompanying departures from ideality in ion radius ratio. a) Highly correlated uniaxial displacements of undersized Ti<sup>4+</sup> cation that result in a tetragonal variant of BaTiO<sub>3</sub> ( $t = 1.059$ ), stable below the Curie temperature but reverting to b) an average-cubic ideal structure above the Curie temperature when the directions of the displacement become uncorrelated. c) Tilting of the [ZrO<sub>6</sub>] octahedra in CaZrO<sub>3</sub> ( $t = 0.914$ ), typical of non-ideal perovskites with overlarge B cations and tolerance parameters  $0.9 < t < 1.0$ , that results in orthorhombic symmetry.

cubic structure and the splitting of certain diffraction peaks (*e.g.* those of the family  $\{h00\}$ ) that would have arisen from crystallographically equivalent planes in the cubic system. They are also responsible for an intriguing array of unusual electrical properties (ferroelectricity, piezoelectricity [BaTiO<sub>3</sub>, Pb(Zr,Ti)O<sub>3</sub>], electrostriction [Pb(Mg,Nb)O<sub>3</sub>, fast ion conduction [LaMnO<sub>3</sub>]) and magnetic properties (magnetoresistance

[(La,Ca)MnO<sub>3</sub>, (La,Sr)CoO<sub>3</sub>]. The cubic→tetragonal transformation temperature corresponds to the Curie temperature, below which ferroelectric behavior appears.

Even in SrTiO<sub>3</sub>, the ideal cubic perovskite arrangement is stable as a sort of “average” structure only above –55° C. As the temperature is lowered below the critical temperature, SrTiO<sub>3</sub> undergoes an increasing tetragonal distortion, similar to that of room-temperature BaTiO<sub>3</sub> and PbTiO<sub>3</sub> (Fig. 4a) whose own critical temperatures for the cubic→tetragonal transformation are 130° C and 490 °C, respectively.

### *X-ray Diffraction*

A periodic arrangement of atoms, such as that found in a crystal, will give rise to constructive interference of scattered (“diffracted”) radiation having a wavelength  $\lambda$  comparable to or smaller than the periodicity  $d$  when Bragg’s law<sup>5</sup> is satisfied,

$$n \lambda = 2d \sin \Theta/2 , \quad (2)$$

where  $n$  is an integer and  $\Theta$  is the angle of between the initial wave incident along direction  $\mathbf{k}$  and the scattered wave departing along direction  $\mathbf{k}'$ . The magnitude of both wave vectors is given by  $|\mathbf{k}| = |\mathbf{k}'| = 1/\lambda$ . The scattering angle  $\Theta$  can also be defined by a scattering vector

$$\mathbf{k} = \mathbf{k}' - \mathbf{k} = 2 (\sin\Theta/2)/\lambda = 2 (\sin\theta)/\lambda \quad (3)$$

where  $\theta = \Theta/2$ ,  $\theta = \theta_B$  at the Bragg condition, and  $\theta_B$  is known as the Bragg angle. Hard X-rays ( $\lambda \sim 0.1$  nm) comprise electromagnetic radiation that satisfies the wavelength criterion for structure investigation at the atomic level ( $d \sim 0.1$  nm) and is scattered sufficiently strongly by atoms (about 1 part in  $10^4$ ) to provide a practical tool for materials structure identification. Bragg’s law (2) tells us necessary conditions for diffraction, but provides no information regarding **intensities** of the constructive maxima, which are necessary information if we are to deduce the details of atomic structure. In order understand the relationship between structural chemistry of solids and the intensity of diffracted X-rays, a more rigorous approach to diffraction must be pursued<sup>5</sup>, an intuitive but non-rigorous version of which follows.

For a one-dimensional array of atoms spaced  $a$  apart (Fig. 6), the condition for constructive interference can be determined from the phase shift of the diffracted wave scattered from each atom, as deduced from the difference in path lengths traveled by incident and diffracted waves from a common initial incident wave front.

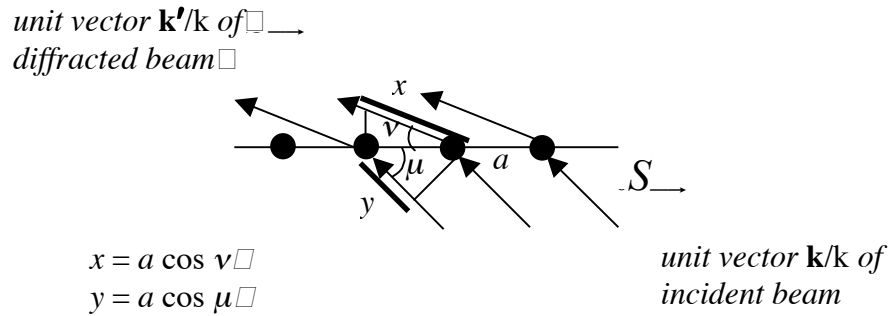


Fig. 6. Geometry for constructive interference from a one-dimensional array of atoms spaced  $a$  apart.

The total path difference  $x - y$ , deduced by geometry from Fig. 6, must be equal to an integer multiple of the wavelength  $\lambda$  at the Bragg condition for constructive interference

$$x - y = a \cos \nu - a \cos \mu = (\mathbf{k}'/k - \mathbf{k}/k) \cdot \mathbf{a} = h\lambda \quad (4)$$

where  $h$  is an integer and the scattering angle  $\Theta = \mu - \nu$ . By extrapolation to three dimensions, with respective atom spacings  $\mathbf{a}$ ,  $\mathbf{b}$  and  $\mathbf{c}$ , the condition for constructive interference becomes

$$\begin{aligned}
 \mathbf{k} \cdot \mathbf{a} &= h \\
 \mathbf{k} \cdot \mathbf{b} &= k \\
 \mathbf{k} \cdot \mathbf{c} &= l
 \end{aligned} \quad (5)$$

where  $h$ ,  $k$  and  $l$  are the Miller indices of families of parallel planes that contain the atoms.

If a set of such identical parallel planes, whose interplanar spacing is  $d$ , is oriented normal to the horizontal axis of Fig. 6, so that the spacing vector  $\mathbf{d}$  is along that axis, then the condition (5) becomes

$$\mathbf{k} \cdot \mathbf{d} = h \quad (5')$$

Using the definition (3) for the scattering vector  $\mathbf{k}$ , (5') may be rewritten  $2\sin\theta/\lambda \cdot d = h$ , or

$$h \lambda = 2d \sin \Theta/2 , \quad (2')$$

which is identical to Bragg's law (2) with  $n = h$  and  $\mathbf{k}$  aligned along  $\mathbf{d}$ . The scattering maxima are frequently (but inaccurately) called “reflections” because, oriented in the Bragg condition, these planes appear to act as mirrors for the radiation at discrete angles  $\theta_B$  that from the diffraction geometry can be shown to represent simultaneously the angles of both incidence onto and reflection from these planes at the Bragg condition. A vector  $\mathbf{g}$  oriented along  $\mathbf{d}$  with magnitude  $1/d$ —known as a reciprocal space vector because, like  $\mathbf{k}$ ,  $\mathbf{k}'$  and  $\mathbf{k}$ , it has dimensions of reciprocal length—can be used to rewrite (5) as

$$\mathbf{k} = \mathbf{g} \quad (5'')$$

called the Laue condition, after the German physicist Max von Laue, who first set out the formal theory of X-ray diffraction from crystals in 1912.

The amplitude scattered by an atom is called the atomic scattering amplitude. X-rays are electromagnetic field waves that interact with the electrically charged constituents of an atom (electrons, protons) and most significantly with the less massive electrons of an atom. The scattered X-ray amplitude is usually referenced to the amplitude scattered by a single electron as the **atomic scattering factor**  $f_n$ , which is proportional to the number of electrons in an atom, and thus to the atomic number  $Z$  of atom  $n$ . Hence, atoms of higher  $Z$  scatter more strongly than do lighter elements. The atomic scattering factor is a function of  $\mathbf{k}$  and thus, from (3), of  $\Theta$  and  $\lambda$  (Fig. 7). For  $\lambda \sim$

0.1 nm X-rays, the scattered amplitude is reduced by half at scattering angles  $\Theta = 2\theta \sim 100^\circ$ .

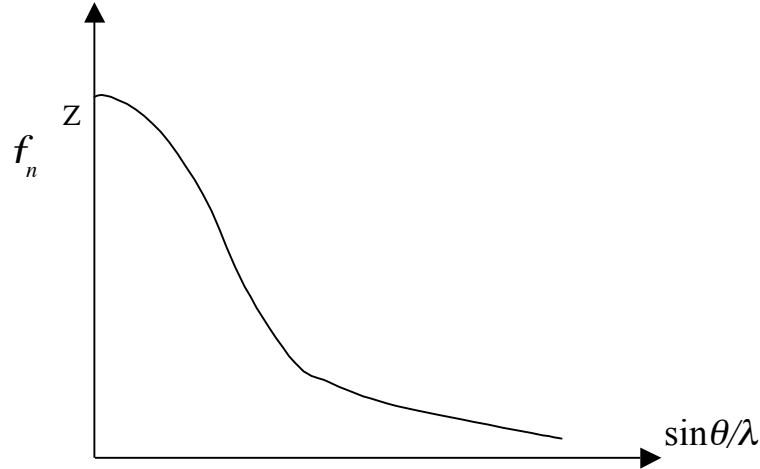


Fig. 7. Variation of atomic scattering factor  $f$  with scattering angle.

For non-monatomic solids, or for a non-primitive choice of unit cell, a periodic array of unit cells may be substituted for atoms in Fig. 6, with the same Bragg result (2). The amplitude scattered from a single unit cell having  $M$  atoms is proportional to the **structure factor**  $F(\mathbf{k})$ , defined as

$$F(\mathbf{k}) = \sum_{n=1}^M f_n \exp(2\pi i \mathbf{k} \cdot \mathbf{r}_n) \quad (6)$$

where

$$\mathbf{r}_n = x_n \mathbf{a} + y_n \mathbf{b} + z_n \mathbf{c} \quad (7)$$

is the atomic position vector for the  $n$ th atom in the unit cell and  $(x_n, y_n, z_n)$  are the atomic position coordinates.

Substituting the atomic positions  $\mathbf{r}_n$  from (7) into the structure factor (6), and using (5) to represent the crystal orientation at the Bragg condition with  $\mathbf{a}$ ,  $\mathbf{b}$  and  $\mathbf{c}$  representing the unit cell vectors

$$F(\mathbf{k}) = \sum_{n=1}^M f_n \exp [2\pi i (hx_n + ky_n + lz_n)] \quad (8)$$

or

$$F_{hkl} = \sum_{n=1}^M f_n \exp [2\pi i (hx_n + ky_n + lz_n)] \quad (9)$$

For example, for a monatomic body-centered cubic structure (Fig. 8) there are two atoms per unit cell, located at  $(0,0,0)$  and  $(1/2,1/2,1/2)$ .

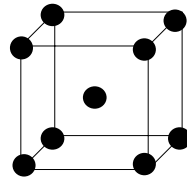


Fig. 8. Monatomic body-centered cubic (non-primitive) unit cell with atoms located at positions  $(0,0,0)$  and  $(1/2,1/2,1/2)$ .

Expanding the structure factor for the unit cell results in the relationship

$$F_{hkl} = f \exp[2\pi i(0)] + f \exp[2\pi i (h/2 + k/2 + l/2)] = f + f \exp[\pi i(h + k + l)] \quad (10)$$

yielding

$$\begin{aligned} F_{hkl} &= 2f && \text{for } h+k+l = \text{even} \\ F_{hkl} &= 0 && \text{for } h+k+l = \text{odd.} \end{aligned} \quad (11)$$

The coherently scattered *intensity* is related to the structure factor by

$$\begin{aligned} I_{\text{coh}} &\propto F F^* = |F_{hkl}|^2 = 4f^2 && \text{for } h+k+l = \text{even} \\ I_{\text{coh}} &= 0 && \text{for } h+k+l = \text{odd} \end{aligned} \quad (12)$$

where  $F^*$  represents the complex conjugate of  $F$ . Note that the *total* coherent intensity will be a sum of the contributions from all unit cells in the crystal. For a body-centered cubic crystal, reflections from planes with Miller indices where  $h+k+l$  is an odd integer will be absent from the diffraction pattern, while reflections from  $\{110\}$ ,  $\{200\}$ ,  $\{211\}$ , *etc.* with  $h+k+l$  an even integer will all be present, reducing in intensity as  $h+k+l$  (and hence  $2\theta$ ) increases (Fig. 9)

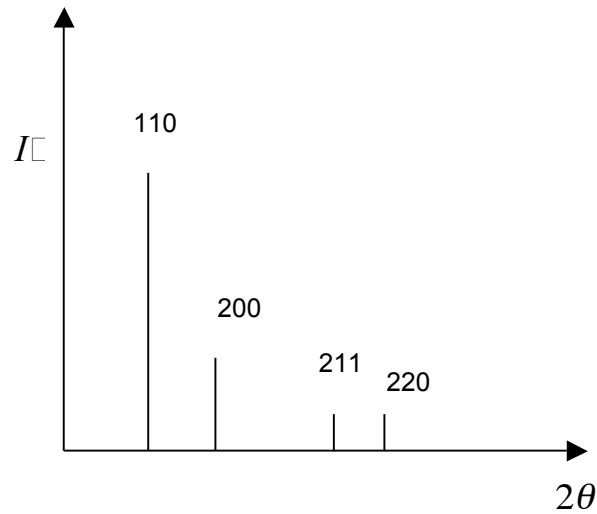


Fig. 9. Discretely-peaked coherent scattering intensity from a body-centered cubic crystal, with peaks indexed with Miller indices of “reflecting” planes.

In the heuristic case considered, constructive interference occurs only at the exact Bragg angle and the  $I$  vs.  $2\theta$  plot exhibits sharp lines of intensity that, mathematically, are  $\delta$ -functions. In reality, Bragg diffraction peaks exhibit finite breadth, due both to instrumental and material effects, and the number of unit cells scattering is proportional to the square root of the integrated area under the broadened peak. An important source of line broadening in polycrystalline materials is finite crystal size. In crystals of finite dimensions, there is incomplete destructive interference of waves scattered from angles slightly deviating from the Bragg angle. If we define the angular width of a peak as

$$B = 1/2 (2\theta_1 - 2\theta_2), \quad (13)$$

then the average crystal size  $w$  can be estimated from the Scherrer formula<sup>6</sup> as:

$$w = 0.9\lambda/B\cos\theta_B \quad (14)$$

A more elegant treatment<sup>7</sup> shows the peak width  $B$  to be, mathematically, the Fourier transform in  $\mathbf{k}$ -space of the crystal size  $w$ . Excessive broadening of diffraction peaks from *very* fine powders can prove problematical for distinguishing closely-spaced peaks.

Interplanar spacings  $d_{hkl}$  can be calculated for different  $hkl$  planes from fixed geometric relationships for a given crystal system with unit cell length parameters  $a$ ,  $b$  and  $c$  and (in the case of the monoclinic system) the characteristic angle  $\beta$  included between  $a$  and  $c$  (Table 5).

Table 5. *Planar Spacings d in Five Crystal Systems*

Cubic:	$1/d^2 = (h^2 + k^2 + l^2)/a^2$
Orthorhombic:	$1/d^2 = h^2/a^2 + k^2/b^2 + l^2/c^2$
Tetragonal:	$1/d^2 = (h^2 + k^2)/a^2 + l^2/c^2$
Hexagonal:	$1/d^2 = 4/3 [(h^2 + hk + l^2)/a^2] + l^2/c^2$
Monoclinic:	$1/d^2 = (1/\sin^2\beta) [h^2/a^2 + k^2 \sin^2\beta/b^2 + l^2/c^2 - 2hl \cos\beta/ac]$

### *Experimental Procedure*

You will be supplied with powders of the following six compounds: CaTiO<sub>3</sub>, SrTiO<sub>3</sub>, BaTiO<sub>3</sub>, PbTiO<sub>3</sub>, PbZrO<sub>3</sub> and CaZrO<sub>3</sub>. Prepare at least five samples for X-ray powder diffractometry, including SrTiO<sub>3</sub>. Process the diffraction patterns acquired by removing the background and then indexing the peaks using JADE<sup>®</sup> software and the Powder Diffraction File. Compare your peaks to those contained in the PDF for the respective ABO<sub>3</sub> compounds.

## Report

In addition to describing your experimental procedure and relating your results to what you have learned about ionic radii and the perovskite structure, your report should include the following:

- A derivation of an expression for the structure factor of  $\text{SrTiO}_3$  and a list of the first ten allowed Bragg maxima in order of increasing diffraction angle.
- A calculation of the lattice parameter of  $\text{SrTiO}_3$  and the ionic radii of  $\text{Sr}^{2+}$  and  $\text{Ti}^{4+}$ , using your X-ray data. Plot the lattice parameter deduced from each indexed peak against diffraction angle  $\Theta = 2\theta$  to deduce the most accurate value for the lattice parameter (why?).
- An explanation of how the size of the A atom in  $\text{ABO}_3$  (with B = Ti) affects the temperature at which the cubic  $\rightarrow$  tetragonal transformation occurs, and an estimate of the cubic  $\rightarrow$  orthorhombic transformation temperature in  $\text{CaTiO}_3$ , using the transformation temperatures for  $\text{SrTiO}_3$ ,  $\text{BaTiO}_3$  and  $\text{PbTiO}_3$  supplied earlier.
- An explanation for any peaks not accounted for in your diffraction patterns.
- An explanation for any observed inconsistency in the tetragonal peak splittings for  $\text{BaTiO}_3$  and  $\text{PbTiO}_3$  with their calculated tolerance parameters. (You may want to consult the notes for Professor Stellacci's counterpart  $\alpha_3$  experiment.)

## References

1. □ V. M. Goldschmidt, *Skifter Norske Videnskaps Akad.*, Oslo I. Mat. Naturv. Kl. No. 8 (1920).
2. □ L. Pauling, *The Nature of the Chemical Bond*, 3<sup>rd</sup> edition (Cornell University Press, 1960).
3. □ R. D. Shannon, *Acta Crystallographica* **A32** (1976) 751.
4. □ W. D. Kingery, H. K. Bowen and D. R. Uhlmann, *Introduction to Ceramics*, 2<sup>nd</sup> edition (John Wiley & Sons, New York, 1976) pp. 81-87.

5. □ Z. L. Wang and Z. C. Kang, *Functional and Smart Materials—Structural Evolution and Structure Analysis* (Springer-Verlag, 1988), Chapter 3: Perovskite and Related Systems,” pp. 93-149; accessible on-line from url: [www.knovel.com/knovel2/Toc.jsp?BookID=906](http://www.knovel.com/knovel2/Toc.jsp?BookID=906).
6. □ B. D. Cullity, *Elements of X-ray Diffraction*, 2<sup>nd</sup> ed. (Addison-Wesley, Reading, MA, 1978), pp. 111-126.
7. □ L. W. Hobbs, “Diffraction from Materials,” accompanying summary text prepared for 3.014, abstracted from L. W. Hobbs, *Diffraction Principles and Materials Applications* (Case Western Reserve University, Cleveland, OH, 1981).